Origin of Hund's multiplicity rule in singly-excited helium: Existence of a conjugate Fermi hole in the lower spin state

Tokuei Sako*
Laboratory of Physics, College of Science and Technology, Nihon University, 7-24-1 Narashinodai, Funabashi, 274-8501 Chiba, Japan

Josef Paldus†
Department of Applied Mathematics, University of Waterloo, Waterloo, Ontario N2L 3G1, Canada

Atsushi Ichimura‡
Institute of Space and Astronautical Science, JAXA, Sagamihara 229-8510, Japan

Geerd H. F. Diercksen§
Max-Planck-Institut für Astrophysik, Karl-Schwarzschild-Strasse 1, D-85741 Garching, Germany
(Dated: June 14, 2011)

The origin of Hund's multiplicity rule in the low-lying excited states of the helium atom has been studied by considering the two-dimensional helium atom. The internal part of the full configuration interaction wave functions for the $(2s)$ and $(2p)$ singlet-triplet pairs of states has been extracted and visualized in the three-dimensional internal space (r_1,r_2, ϕ_-). The internal wave function of the singlet states *without* electron repulsion has a significant probability around the origin of the internal space while the corresponding probability of the triplet wave function is negligible in this region due to the presence of a Fermi hole. The electron-electron repulsion potential has been visualized also in the internal space. It manifests itself by three striking poles penetrating exactly into the spatial region defined by the Fermi hole. Because of the existence of these strong potential poles in the vicinity of the Fermi hole a major part of the singlet probability migrates out of this region. In contrast, the corresponding triplet wave function is less affected by these poles due to the presence of the Fermi hole. The singlet probability is shown to migrate from its original region close to the origin to a region far away where either r_1 or r_2 are large. This results in a more diffuse electron density distribution and a smaller electron repulsion energy of the singlet state than of the corresponding triplet state. The mechanism of the evolution of the singlet probability towards the region of large r_i $(i = 1, 2)$ in the presence of the electron repulsion potential has been rationalized on the basis of a new concept called *conjugate Fermi hole*.

PACS numbers: 31.10.+z, 31.15.A-, 32.10.-f

I. INTRODUCTION

Hund's rules [1–4], initially derived empirically in atomic spectroscopy of the pre-quantum-mechanical era, consist of three rules that predict the ordering of the energy levels possessing different spin and orbital angular momentum quantum numbers. These three rules, particularly the first rule concerning the spin multiplicity, proved to be almost universally valid not only for atomic systems [5–8] but also for molecules [9, 10] and 'artificial atoms' [11–13]. The first Hund rule states that among the different spin states belonging to the same orbital configuration it is the highest spin state that has the lowest energy. In the intervening years since the formulation of these rules numerous authors endeavored to provide their theoretical underpinning [14–32]. More recently, similar attention has been paid to the role of Hund rules in quantum dots or artificial atoms [33, 34].

By using a minimum-basis-set frozen-orbital independent particle model approximation, Slater [14] was the first to show that higher spin states weaken the inter-electronic repulsion so that the energy difference between the singlet and triplet states of the two-electron atom He can be ascribed to the difference in their two-electron energies [6, 7]. This explanation was then employed in various studies until Davidson pointed out the importance of orbital relaxation. He showed [15, 16] that at the Hartree-Fock level the two-electron energy contribution is actually larger in the high-spin state while it is the nuclear attraction term that is responsible for the lowering of the triplet relative to the singlet state in the singly-excited states of the helium atom. This implies that the reason for a lower energy of the triplet state relative to the corresponding singlet state cannot be due to a decrease in the electron-electron interaction potential. Instead, it must be ascribed to a more compact electron

*Electronic address: sako@phys.ge.cst.nihon-u.ac.jp; URL: http://www.phys.ge.cst.nihon-u.ac.jp/~sako/
†Electronic address: paldus@uwaterloo.ca; URL: http://www.math.uwaterloo.ca/~paldus/
‡Electronic address: ichimura@isas.jaxa.jp
§Electronic address: ghd@mpa-garching.mpg.de; URL: http://www.mpa-garching.mpg.de/mol_physics/index.shtml

density distribution of the triplet state which then results in a much larger energy decrease due to the nuclear attraction potential that compensates the energy increase in the electron-electron repulsion potential [10, 17, 19–25].

Following Davidson's paper a number of studies evaluated one-electron and two-electron energies with improved accuracy confirming Davidson's conclusion for neutral atomic species [30, 31] and provided additional insight into the problem. The same nature of the one- and two-electron components in the singlet and triplet excited states of He was shown to hold even when correlation effects are accounted for [18, 32]. Recently, a very thorough study of these effects has been carried out by Oyamada *et al.* [32] to which we refer the reader for an excellent overview of the literature concerning this problem.

Nonetheless, there still exists an ambiguity concerning the reason why the triplet state has a more compact electron-density distribution than the corresponding singlet state. We recall here, for example, the puzzling behavior of various global quantities, like $\langle 1/r_{12}\rangle$, $\langle r_{12}\rangle$, $\langle r_{12}^2\rangle$, of the He atom as observed by Katriel [19–22] and the analysis of intracule and extracule density functions by Thakkar *et al.* [26–28]. Further, it was argued [29] that the Fermi hole induces a larger repulsion between electrons with parallel spins that results in a larger average inter-electron angle $\angle(\mathrm{e}{-}\alpha{-}\mathrm{e})$ of the triplet electrons than of the singlet electrons. This allowes the triplet electrons to be closer to the nucleus due to 'less screening' of the nuclear charge [25]. On the other hand, very recently it has been shown by Sajeev *et al.* [33] that angular electron correlation is not important in the singly-excited states of helium in order to yield its energy levels accurately, although the triplet electrons may require to be angularly correlated to some extent in order to have a larger inter-electron angle than the corresponding singlet electrons.

In our earlier study [34] the origin of Hund's multiplicity rule in two-electron artificial atoms was studied. The mechanism for a more compact electron density distribution in the triplet states was clarified by examining the nodal pattern of the wave functions in the internal space. Motivated by this analysis the present study examines the internal wave functions of the He atom in order to provide a deeper understanding of the workings of the first Hund rule. For this very reason a two-dimensional model of the helium atom has been imployed since the reduced dimension of the problem makes it possible to gain a more thorough insight into the reasons for the validity of the first Hund rule.

II. THEORETICAL MODEL AND COMPUTATIONAL METHOD

In the present study the spatial degrees of freedom of each of the two electrons in the helium atom are confined to a two-dimensional xy plane. In the case of the real three-dimensional helium atom this xy plane, as defined by the position of the two electrons and the nucleus, can freely rotate about the three principal axes of inertia by the Euler angles (α, β, γ). In the two-dimensional helium atom this rotation is limited to the rotation about the axis that is normal to the xy plane. Although this two-dimensional helium atom represents a simplified model, it has all the characteristic features of the energy spectrum of the real 3D helium atom as will be shown in the next section. For example, the same energy ordering of the $(1s)\ ^1S < (2s)\ ^1S < (2p)\ ^1P < (3s)\ ^1S < (3d)\ ^1D < (3p)\ ^1P, \cdots$ states for the singlet manifold and of the $(2s)\ ^3S < (2p)\ ^3P < (3s)\ ^3S < (3p)\ ^3D < (3d)\ ^3D, \cdots$ states for the triplet manifold follows the Hund multiplicity rule. By reducing the number of the degrees of freedom the internal part of the wave functions can be easily visualized allowing an unambiguous manifestation of the origin of the Hund rule.

TABLE I: Summary of parameters for the atomic basis set of the two-dimensional helium atom.

l	m_l	$\zeta_{\mathrm{max},l}$	$\zeta_{\mathrm{min},l}$
0	23	3000.0	0.0002
1	12	20.0	0.001
2	9	8.0	0.001
3	5	1.0	0.01

The electronic Hamiltonian for the two-dimensional helium model has the form

$$\mathcal{H} = -\frac{1}{2}\sum_{i=1}^{2}\vec{\nabla}_i - \sum_{i=1}^{2}\frac{Z}{|\vec{r}_i|} + \frac{1}{|\vec{r}_1 - \vec{r}_2|}, \qquad (1)$$

where $Z = 2$ and $\vec{r}_i = (x_i, y_i)$ for $i = 1, 2$. A $[23s12p9d5f]$ basis set of two-dimensional Cartesian Gaussian-type functions of the form

$$\chi^{\vec{a},\zeta}(\vec{r}) = x^{a_x} y^{a_y} \exp[-\zeta(x^2 + y^2)] \qquad (2)$$

has been used. Following the quantum chemical convention these functions are classified as of s-, p-, d-, and f-type for $l = a_x + a_y = 0$, 1, 2 and 3, respectively. The exponents of the Gaussian functions have been generated by using the geometrical formula [35, 36] (see also Ref. [37] for further information)

$$\zeta_{j,l} = \alpha_l \beta_l^{j-1},\ j = 1, 2, \cdots, m_l. \qquad (3)$$

The minimum and maximum exponents, $\zeta_{\mathrm{min},l}$ and $\zeta_{\mathrm{max},l}$, and the number of components m_l for each l-shell are listed in Table I. For the calculation of He-like atomic ions, like Li^+, Be^{2+}, $\cdots$ etc., presented in Sec. III E all exponents used for the basis set of the He atom have been scaled as $\zeta\times(Z/2)^2$, where Z represents the nuclear charge of the atomic species.

The eigenfunctions $\Psi_{\mathrm{FCI}}(\vec{r}_1, \vec{r}_2)$, $\vec{r}_i = r_i(\cos\phi_i, \sin\phi_i)$, $i = 1, 2$, and the corresponding energies for the relevant states have been obtained by diagonalizing the

full configuration interaction (FCI) Hamiltonian matrix. Since the interelectronic coordinate r_{12} depends only on $r_1 \equiv |\vec{r}_1|$, $r_2 \equiv |\vec{r}_2|$ and the phase difference $\Phi_- \equiv (\phi_1 - \phi_2)/2$, the complementary phase coordinate $\Phi_+ = (\phi_1 + \phi_2)/2$ is associated with the total angular momentum $L = l_1 + l_2$. Therefore we can write $\Psi_{\rm FCI}(\vec{r}_1, \vec{r}_2) = \Psi_{\rm int}(r_1, r_2, \Phi_-) \exp(\pm i\Phi_+ L)$, where $\Psi_{\rm int}$ represents the *internal wave function*. The square norm of $\Psi_{\rm int}$ is equivalent to $|\Psi_{\rm FCI}|^2$ since $|\exp(\pm i\Phi_+ L)| = 1$. Thus $|\Psi_{\rm int}|^2$ provides the relevant information for each state.

Since real arithmetic has been employed in the computations the diagonalization code generates some linear combination of eigenvectors that are associated with doubly degenerate eigenvalues when $L \neq 0$. In order to obtain the internal wave function from the resulting eigenvectors the square-average of the probability amplitudes of these doubly-degenerate eigenvectors have been computed.

To normalize $|\Psi_{\rm int}|^2$ we have to perform integration on the ignorable phase coordinates Φ_+. For this purpose we introduce new coordinates, namely $\phi_+ \equiv \Phi_+ - \pi = \frac{1}{2}(\phi_1 + \phi_2) - \pi$ and $\phi_- \equiv \Phi_- = \frac{1}{2}(\phi_1 - \phi_2)$, so that $\phi_1 = \phi_+ + \phi_- + \pi$ and $\phi_2 = \phi_+ - \phi_- + \pi$. Focusing on the angular part of the fourfold integral over r_1, r_2, ϕ_-, and ϕ_+, we consider

$$I \equiv \int_0^{2\pi} d\phi_1 \int_0^{2\pi} d\phi_2 F(\phi_-), \tag{4}$$

where we have written for simplicity $F(\phi_-) \equiv |\Psi_{\rm int}(r_1, r_2, \phi_-)|^2$. We carry out a transformation to the new coordinates ϕ_+ and ϕ_- yielding

$$\begin{aligned} I &= 2\left[\int_0^{\pi} d\phi_- \int_{\phi_- - \pi}^{\pi - \phi_-} d\phi_+ F(\phi_-) + \int_{-\pi}^{0} d\phi_- \int_{-(\pi+\phi_-)}^{\pi+\phi_-} d\phi_+ F(\phi_-)\right] \\ &= 4\int_{-\pi}^{\pi} d\phi_- (\pi - |\phi_-|) F(\phi_-). \end{aligned} \tag{5}$$

In the second integral we have expressed $(\pi + \phi_-)$ as $(\pi - |\phi_-|)$ since $\phi_- \leq 0$ and have accounted for the appropriate Jacobian by the factor 2. Finally, we can write the correctly normalized probability density for the internal wave function as

$$|\Psi_{\rm int}^{\rm norm}(r_1, r_2, \phi_-)|^2 = 4(\pi - |\phi_-|)|\Psi_{\rm int}|^2, \tag{6}$$

so that the normalization integral becomes

$$\int_0^{\infty} r_1 dr_1 \int_0^{\infty} r_2 dr_2 \int_{-\pi}^{\pi} d\phi_- |\Psi_{\rm int}^{\rm norm}(r_1, r_2, \phi_-)|^2 = 1. \tag{7}$$

For the S states with $L = 0$ the FCI wave function $\Psi_{\rm FCI}(\vec{r}_1, \vec{r}_2)$ does not depend on Φ_+ (or ϕ_+) so that the internal wave function can be obtained from Eq. (6) by replacing $\Psi_{\rm int}$ by $\Psi_{\rm FCI}$.

To understand the presence of the factor $2(\pi - |\phi_-|)$ we observe that the square integration domain $0 \leq \phi_i \leq 2\pi$, $i = 1,2$ for ϕ_1 and ϕ_2 is transformed into a square domain with vertices $(\phi_+, \phi_-) = (-\pi, 0)$, $(0, \pm\pi)$, and $(\pi, 0)$. Thus, for a given fixed value of ϕ_-, the second variable ϕ_+ cannot take on all values of the interval $-\pi \leq \phi_+ \leq \pi$ but only those that are inside the triangle $-(\pi - \phi_-) \leq \phi_+ \leq (\pi - \phi_-)$ for $\phi_- \geq 0$ and, similarly, for $\phi_- \leq 0$. This fact will reappear in the next section.

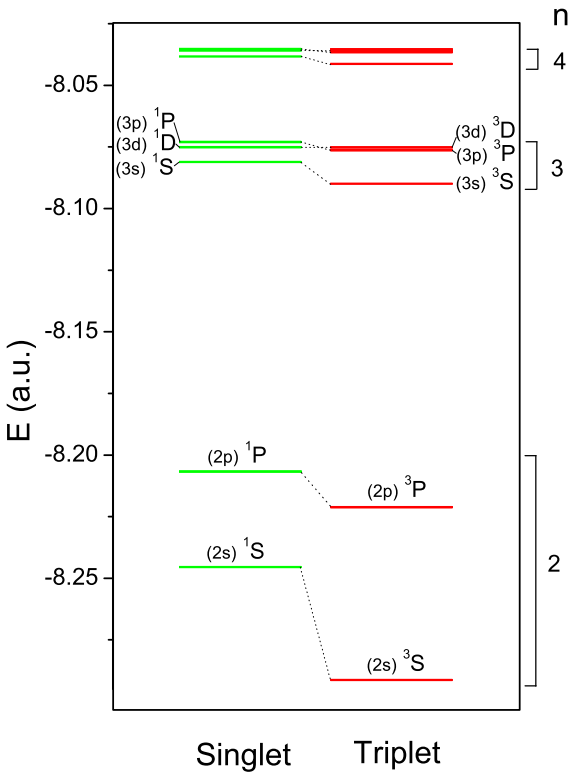

FIG. 1: (Color online) Energy-level diagram for the low-lying excited states of the two-dimensional helium atom obtained from the FCI calculation by using an $[23s12p9d5f]$ basis set. The singlet and triplet levels are colored in green (light grey) and red (dark grey), respectively. The number n on the right-hand-side of the figure specifies the principal quantum number. The correspondence between singlet-triplet pairs is indicated by dotted lines.

III. RESULTS AND DISCUSSION

A. Energy levels and electron density

The energy spectrum of the low-lying excited states of the two-dimensional helium atom obtained from the FCI calculation is displayed in Fig. 1. This energy spectrum possesses the same qualitative features as the spectrum of the actual 3D helium atom. The singlet-triplet splitting is the largest for the S states and decreases as the total angular momentum increases. The magnitude of

TABLE II: Energy differences (in 10^{-3} hartree) of the total, one-electron, and two-electron energies ΔE, ΔE_1, and ΔE_2 between the singlet-triplet pairs for the low-lying excited states of the two-dimensional helium atom.

state	ΔE	ΔE_1	ΔE_2
1s2s	45.888	83.823	−37.935
1s2p	14.483	49.483	−35.000
1s3s	8.822	17.748	−8.926
1s3p	3.342	11.232	−7.890
1s3d	0.015	0.086	−0.071

these splittings monotonically decreases with increasing principal quantum number n. We note that even the reverse order of the energy levels for the singlet P states that is characteristic of He-like atoms, is also found in the energy spectrum of the 2D He in Fig. 1. This means that the P state has the largest energy among the states belonging to the same n shell in the singlet manifold, e.g., $(3s)\ ^1S < (3d)\ ^1D < (3p)\ ^1P$, etc.. The only apparent difference between the energy spectra of the 2D and 3D helium atoms lies in their absolute energy values. The $(2s)\ ^1S$ excited state, for example, is located at $E = -2.146$ a.u. for the 3D helium atom but at $E = -8.245$ a.u. for the 2D case. This large negative energy of the 2D helium atom is likely due to the missing zero-point energy in the z direction. The fact that in the 3D case the electrons are confined not only in the x and y directions but also in the z direction results in an additional energy increase by the amount corresponding to the zero-point energy of the z degree of freedom.

The total energies ${}^SE$ and their one- and two-electron components, ${}^SE_1$ and ${}^SE_2$, respectively, where $S \equiv 1$ or 3 specifies the spin multiplicity, have been calculated for the five lowest singlet-triplet pairs of states which we label as $(2s)$, $(2p)$, $(3s)$, $(3p)$, and $(3d)$. The differences between the respective singlet and triplet states, i.e., $\Delta E \equiv {}^1E - {}^3E$, $\Delta E_1 \equiv {}^1E_1 - {}^3E_1$, and $\Delta E_2 \equiv {}^1E_2 - {}^3E_2$, are summarized in Table II. In all cases the difference of the two-electron energies ΔE_2 is negative. This indicates that the triplet is associated with a larger expectation value of the two-electron energy than the corresponding singlet as observed for the 3D helium atom. Consequently, the singlet-triplet energy difference ΔE is due to a decrease of the one-electron energy. It should be noted also that the energy difference for the $(3d)$ singlet-triplet pair is very small in comparison to the differences for the $(3s)$ and $(3p)$ pairs. This very small energy difference in the $(3d)$ case is observed also for the 3D helium atom.

The radial electron density distributions for the $(2s)$ and $(2p)$ singlet and triplet states are plotted in Fig. 2. We use a logarithmic scale for the density in order to emphasize small differences between the singlet and triplet electron density distributions. From this figure it is seen that for both the $(2s)$ and $(2p)$ states the electron density distribution for the triplet state, represented by the red (dark grey) curve, is more compact and closer to the origin than for the corresponding singlet state, represented by the green (light grey) line. This implies a larger energy decrease in the nuclear attraction potential for the triplet state than for the singlet state. This again parallels the 3D case [27]. The difference between the singlet and triplet density distributions is less pronounced for the $(2p)$ singlet-triplet pair than for the $(2s)$ singlet-triplet pair. This is consistent with a smaller energy difference ΔE for the $(2p)$ pair in comparison to the $(2s)$ pair as shown in Table II.

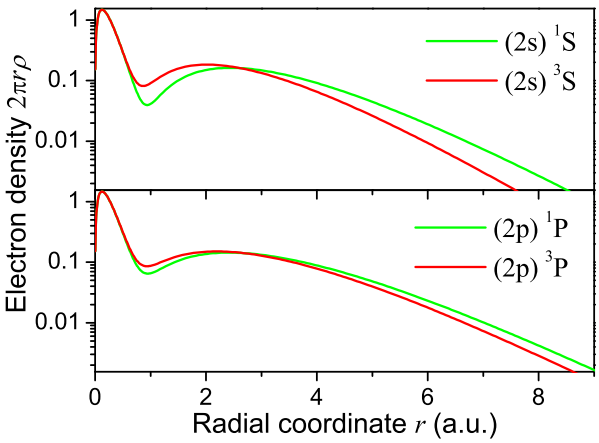

FIG. 2: (Color online) Radial electron density distributions (in logarithmic scale) for the $2s$ singlet-triplet pair of states (upper) and the $2p$ singlet-triplet pair (lower) of the two-dimensional helium atom. The singlet and triplet distributions are colored in green (light grey) and red (dark grey), respectively.

B. Internal wave functions

In order to rationalize the observations made in the preceding section we present in Figs. 3 and 4 the internal wave functions for the $(2s)\ ^1S$ and $(2s)\ ^3S$ pair of states and for the $(2p)\ ^1P$ and $(2p)\ ^3P$ pair, respectively, as an isosurface of their square norm for the value 0.015. In order to assess the role of the electron repulsion we also show in these figures the results obtained with the inter-electronic potential ignored. In the right-handed Cartesian coordinate system used in these figures the three axes x, y, and z correspond to, respectively, the r_1, r_2, and ϕ_- coordinates and cover the spatial region $0 \le r_i \le 5.0$ for $i = 1,2$ and the angular region $-\pi \le \phi_- \le \pi$ (we note that in the following figures the scale of the ϕ_- axis is labeled numerically in radians rather than fractions of π, e.g., $\pi/2$, etc.). From Fig. 3 a clear difference between the singlet and triplet wave functions of the $(2s)$ pair in the vicinity of $(r_1, r_2) = (0, 0)$ is apparent. The singlet

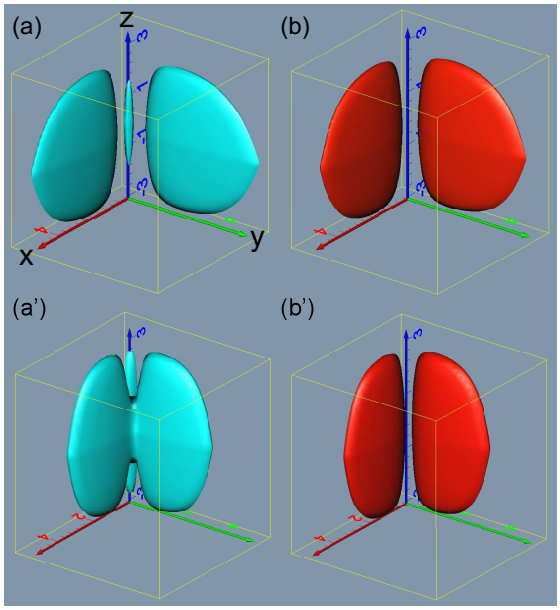

FIG. 3: (Color online) Isosurfaces of the probability density for the internal wave functions for the $(2s)$ singlet-triple pair of the helium atom: (a) $(2s)\ ^1S$ and (b) $(2s)\ ^3S$. The isosurfaces in the bottom part of the figure, (a') and (b'), are obtained by ignoring the electron repulsion. The square-norm of the displayed surface is 0.015. In all four figures the right-handed Cartesian coordinates, x, y and z, indicated in (a) correspond, respectively, to r_1, r_2 and ϕ_-.

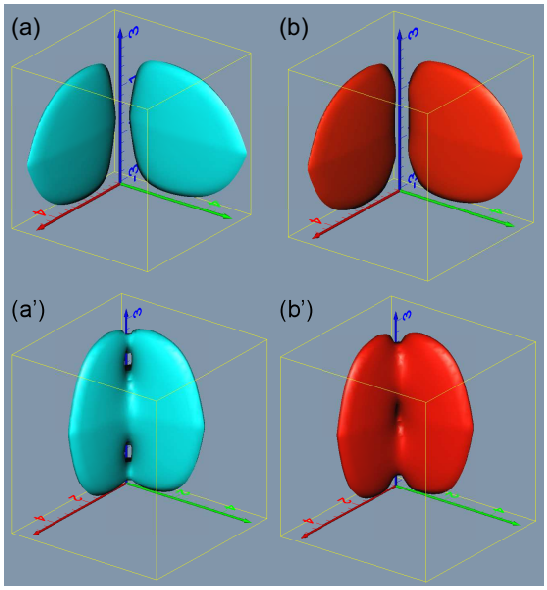

FIG. 4: (Color online) Isosurfaces of the probability density for the internal wave functions for the $(2p)$ singlet-triple pair of the 2D helium atom: (a) $(2p)\ ^1P$ and (b) $(2p)\ ^3P$. The isosurfaces in the bottom part of the figure, (a') and (b'), are obtained by ignoring the electron repulsion. See the caption of Fig. 3 for further details.

wave functions obtained with and without electron repulsion have a significant probability distribution in this region while the triplet wave functions have a node in the region. This node is the so-called Fermi hole arising due to the fact that two electrons with the same spin cannot occupy the same spatial position. The interchange of the coordinates of electrons 1 and 2, $(x_1, y_1) \leftrightarrow (x_2, y_2)$, corresponds to the coordinate transformation $r_1 \leftrightarrow r_2$ and $\phi_- \leftrightarrow -\phi_-$ in the internal space. Due to the Pauli principle the triplet wave functions for the $(2s)\ ^3S$ state (cf. Fig. 3(b)) must change sign when exchanging their left and right lobes with respect to the plane defined by the equation $r_1 = r_2$, while a change of sign is not required for the singlet wave functions.

The above results for the left and right lobes of both the singlet and triplet wave functions of the $(2s)$ pair can be easily interpreted in terms of the one-electron orbitals. In a zeroth order approximation the orbital part of these wave functions can be expressed as a single determinant

$$\Psi^{\pm}_{2s} = \frac{1}{\sqrt{2}}[\psi_{1s}(\vec{r}_1)\psi_{2s}(\vec{r}_2) \pm \psi_{2s}(\vec{r}_1)\psi_{1s}(\vec{r}_2)], \qquad (8)$$

where Ψ^{+}_{2s} and Ψ^{-}_{2s} correspond to, respectively, the singlet and triplet state. Strictly speaking, the orbitals ψ_{1s} and ψ_{2s} are distinct for the singlet and triplet states when independently optimized. In particular, the ψ_{2s} orbital of the singlet is more diffuse than that of the triplet as also suggested by the radial electron density distributions in Fig. 2 [15, 16]. However, the interpretation given here concerning the left and right lobes of the internal wave functions does not depend on the fine details of the orbitals. The wave functions of Eq. (8) involve two terms, namely $\psi_{1s}(\vec{r}_1)\psi_{2s}(\vec{r}_2)$ and $\psi_{2s}(\vec{r}_1)\psi_{1s}(\vec{r}_2)$. The first term represents a contribution in which electrons 1 and 2 are in the $1s$ and $2s$ orbitals, respectively. This implies that the probability distribution along the r_1 axis that is associated with this component is confined to the vicinity of the origin due to the compactness of the 1s orbital, while it extends along the r_2 axis in view of the more diffuse nature of the 2s orbital. Therefore, this part of the wave function is associated with the right lobe of the internal wave functions in Fig. 3 that extends along the r_2 axis. Similarly, the second term $\psi_{2s}(\vec{r}_1)\psi_{1s}(\vec{r}_2)$ is associated with the left lobe extending along the r_1 axis. Internal wave functions involving doubly-excited configurations, such as $(2s)^2$, $(2s)(2p)$, etc., look different since, in this case, both electrons occupy outer orbitals whose average radii are of the same order.

The internal wave functions for the $(2p)$ singlet and triplet pair of states shown in Fig. 4 have a more complicated nodal structure along the ϕ_- axis than those for $(2s)$, particularly for the case when the interelectron potential is ignored: The wave functions (a') and (b') in Fig. 4 have, respectively, two nodes at $\phi_- = \pm\pi/2$ and one node at $\phi_- = 0$ with $r_1 = r_2 \equiv r$ for small r. The presence of these nodes along the ϕ_- axis is due to a nonzero orbital angular momentum of the $(2p)$ states. The mechanism for the appearance of these nodes will be discussed in Sec. III D.

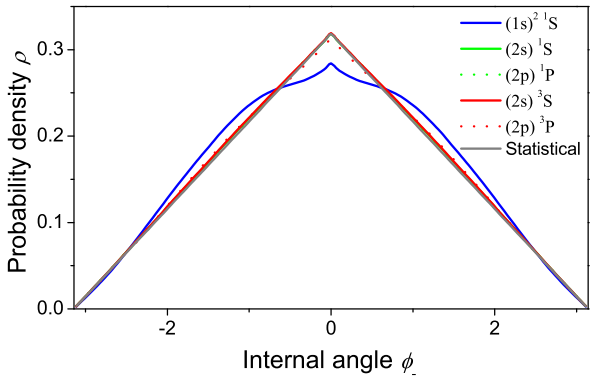

FIG. 5: (Color online) Probability density distributions along the internal angle ϕ_- for the $(2s)$ and $(2p)$ singlet-triplet pairs of states and for the $(1s)$ ground state of the helium atom. The solid and dotted lines indicate $(2s)$ and $(2p)$, respectively; the green (light grey) and red (dark grey) lines indicate singlet and triplet, respectively. The blue (black) curve indicates the $(1s)$ ^1S ground state and the bold light grey line represents the *statistical distribution* defined by $(\pi - |\phi_-|)/\pi^2$.

The angular correlation between the two electrons can be examined by integrating the relevant wave functions over the radial coordinates r_1 and r_2 for a given value of ϕ_-. This corresponds to cutting the wave functions displayed in Figs. 3 and 4 by a plane parallel to the xy plane for a particular value of $z = \phi_-$ and integrating the probability density in this plane by using the volume element $r_1 dr_1 r_2 dr_2$. The resulting probability density as a function of ϕ_- is displayed in Fig. 5 for the studied $(2s)$ and $(2p)$ singlet and triplet states. For comparison, the distribution for the $(1s)^2$ ^1S ground state is also shown in this figure. The probability distributions for the $(2s)$ and $(2p)$ singlet-triplet pairs of states are nearly identical and have a triangular shape peaked at $\phi_- = 0$ that follows closely the *statistical distribution* represented by the grey line. The triangular statistical distribution is given by the factor $(\pi - |\phi_-|)$ in Eq. (6) and normalized so that the integral over ϕ_- is unity. It corresponds to the situation in which both electrons change their polar angles independently over the interval $[0, 2\pi]$. This means that the probability for the two electrons to take a particular inter-electron angle $\angle(\mathrm{e}{-}\alpha{-}\mathrm{e})$, denoted by θ_{12}, is the same for all θ_{12}. This is confirmed by a simple geometrical analysis of the statistical triangular distribution. Since the set of internal angles $\pm\phi_-$ and $\pm(\pi - \phi_-)$ for $0 \leq \phi_- \leq \pi/2$ gives the same value of θ_{12}, summing the probability distribution of Fig. 5 over these four internal angles gives the same value of $2/\pi$ for any θ_{12}. Therefore, since the present result of the angular probability distributions for both $(2s)$ and $(2p)$ pairs closely follows the statistical triangle, the two electrons in the $(2s)$ and $(2p)$ excited states have little preference for their angular configuration. It indicates that they have very small angular correlation. This result is consistent with the recent study that explored the angular correlation in excited states of He by varying angular functions in the basis set that are responsible for the angular correlation [33]. We note, however, that a close examination of the numerical results does reveal some angular dependence for the $(2p)$ singlet-triplet pair of states while it is negligibly small for the $(2s)$ pair.

The situation is different for the ground $(1s)^2$ ^1S state where both electrons occupy the same lowest $(1s)$ orbital. In this case the angular dependence of the probability density significantly deviates from the statistical triangle. It has a smaller probability around $\phi_- = 0$ and a larger one around $\phi_- = \pm\pi/2$ as shown in Fig. 5. These deviations at $\phi_- = 0$ and $\pm\pi/2$ correspond to configurations where the two electrons are on the same and on the opposite sides of the nucleus, respectively. Since in the ground state both electrons occupy the same orbital they strongly avoid each another resulting in the distribution shown in Fig. 5. This feature of the ground state is not unlike that characterizing doubly excited states of He for which it is known [38] that the two electrons try to avoid one another by staying on opposite sides of the nucleus indicating a strong angular correlation. On the other hand, in the case of singly excited states of He with one electron occupying the $1s$ orbital and the other an outer orbital the angular correlation is insignificant, since the $1s$ electron is tightly bound to the nucleus and only slightly affects the outer electron regardless of whether the $1s$ electron is on the same side or on the opposite side of the nucleus.

C. Electron repulsion in the internal space

We recall that the square norm of the internal wave function for the $(2s)$ ^1S state, as obtained when disregarding the interelectronic repulsion [cf. Fig. 3(a')], shows a large probability density in the vicinity of the ϕ_- axis i.e., for $(r_1, r_2) = (0, 0)$. Once the electron repulsion is introduced, however, a major part of the probability density migrates out of this region [cf. Fig. 3(a)]. On the other hand, in case of the corresponding triplet states [cf. Fig. 3 (b) and (b')] the role of the electron repulsion seems to have a smaller effect although the distribution as a whole becomes broader as in the singlet case. In order to better understand the migration of the probability in the singlet case and thus to rationalize the differences between the singlet and triplet wave functions, we have plotted the electron repulsion potential and the difference between the probability density distributions of the singlet and triplet states in Figs. 6 and 7, respectively. The surface of the electron repulsion potential displayed in Fig. 6 represents the region where the potential energy is larger than 3.0 a.u. It has three peaks along the ϕ_- axis at $\phi_- = 0$ and $\pm\pi$ that extend into the $r_1 = r_2$ direction. These internal angles correspond

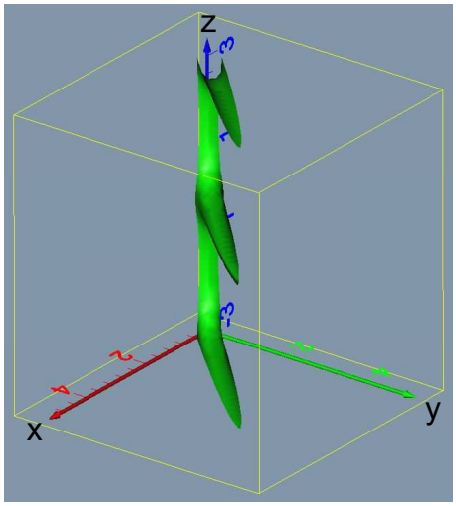

FIG. 6: (Color online) Electron repulsion potential in the internal space (r_1, r_2, ϕ_-). The displayed surface represents the area where the electron repulsion potential energy becomes larger than 3.0 (a.u.). See the caption to Fig. 3 for further details.

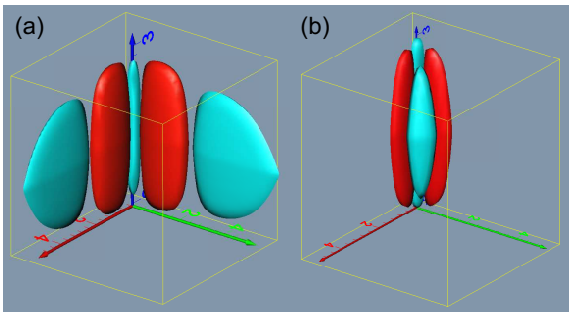

FIG. 7: (Color online) Difference between the probability density distributions of the (2s) ^{1}S singlet state and of (2s) ^{3}S triplet state in the internal space: (a) and (b) correspond to the cases with and without electron repulsion, respectively. The square norm of the displayed surface is 0.005. The blue (right grey) and red (dark grey) surfaces correspond, respectively, to the regions where the probability density of the singlet wave function is larger than that of the triplet wave function and vice versa. See the caption to Fig. 3 for further details.

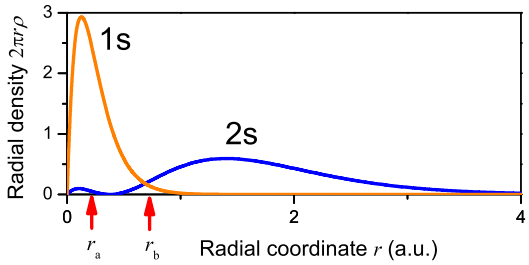

FIG. 8: (Color online) Radial density distribution of the analytical 1s and 2s orbitals of a two-dimensional Coulomb problem with $Z = 2$. The arrows indicate an example of a pair of coordinates (r_a, r_b) delimiting a *conjugate Fermi hole* where the (2s) singlet wave function has a lower probability than the corresponding triplet in the region of small r close to the nucleus.

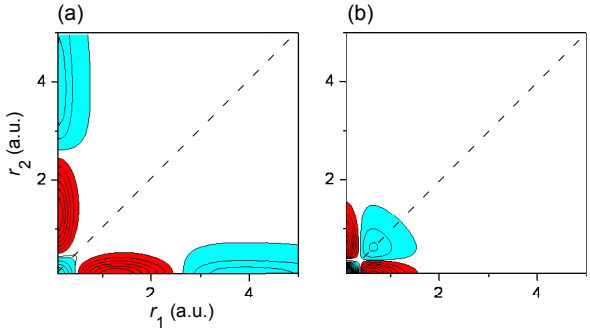

FIG. 9: (Color online) Cross sections at $\phi_- = 0$ of the isosurfaces of the difference between the (2s) singlet and triplet internal probability densities displayed in Fig. 7 (a) and (b). The figures (a) and (b) correspond to the cases with and without electron repulsion, respectively. Along the dotted diagonal line the electron repulsion potential diverges. The blue (light grey) and red (dark grey) contours represent, respectively, the regions where the singlet wave function has a larger probability density than the corresponding triplet and vice versa.

to spatial configurations in which the electron position vectors align parallel to each other. Therefore, the electron repulsion potential diverges along $r_1 = r_2$. Since the potential energy becomes very large in this region, the probability density in it should be small. For this reason the density in the (2s) ^1S state decreases close to the ϕ_- axis when the electron repulsion is accounted for. In the corresponding triplet case there is a node along the ϕ_- axis due to the Pauli principle so that it is less affected by the electron repulsion potential.

In case of the (2p) singlet-triplet pair the singlet and triplet wave functions without the electron repulsion have similar probability distributions along the ϕ_- axis except for the location of their node points as displayed in Fig. 4 (a') and (b'). Since their difference is less pronounced than the (2s) pair the difference between the singlet and triplet states is still smaller when the interelectron potential is accounted for. This is consistent with a smaller energy gap shown in Fig. 1 relative to the (2s) singlet-triplet pair.

D. Emergence of a conjugate Fermi hole

The origin of a more compact electron density distribution and a larger electron repulsion in the triplet state relative to the corresponding singlet of the (2s) pair can

be rationalized by the difference between their probability distributions as obtained with and without the electron repulsion displayed in Fig. 7 (a) and (b), respectively. The blue (light grey) and red (dark grey) surfaces in these figures represent, respectively, the regions in which the singlet wave functions have a larger probability than the corresponding triplet and vice versa. As is apparent from Fig. 7(a) the blue surfaces extend in the direction of increasing r_1 or r_2 coordinates. This implies that the singlet state electron density for large r_1 and r_2 exceeds that of the triplet state as has been noticed already in the upper part of Fig. 2. Yet, *if* there is *no* electron repulsion there is no difference in the probability distributions of the singlet and triplet wave functions in the region of large r as is seen from Fig. 7(b). Therefore, the singlet probability density in the region of large r values must originate in the region of small r where the singlet wave function *without* the electron repulsion has a significant probability density as is seen in Fig. 3(a'). We emphasize that the probability density that migrates from the region of small r values does not accumulate in the nearby red surface region but rather in the distant blue region. The region in which the singlet state has a smaller probability density than the triplet, as represented by the red surfaces in Fig. 7, arises due to the sign change of the outer $2s$ orbital within the region of large overlap with the inner $1s$ orbital. Within a single-determinant approximation the orbital part of the singlet and triplet wave functions has the form as represented by Eq.(8) with + and − corresponding to the singlet and triplet functions, respectively. A subtle difference between the one-electron orbitals for the singlet and triplet states does not affect the following discussion. The $1s$ orbital ψ_{1s} is nodeless while the $2s$ orbital ψ_{2s} has a node as displayed in Fig. 9 where the radial orbital density distributions of the analytical $1s$ and $2s$ orbitals for the two-dimensional Coulomb problem [39] are displayed. For two spatial points, $\vec{r}_a$ and $\vec{r}_b$, (as indicated by the arrows in the figure) that are separated by the nodal point, the square-norm of the singlet wave function $\left|\Psi^{+}_{2s}(\vec{r}_a,\vec{r}_b)\right|^2$ is smaller than that of the triplet $\left|\Psi^{-}_{2s}(\vec{r}_a,\vec{r}_b)\right|^2$ since in the case of the singlet the two terms $\psi_{1s}(\vec{r}_a)\psi_{2s}(\vec{r}_b)$ and $\psi_{2s}(\vec{r}_a)\psi_{1s}(\vec{r}_b)$ are subtracted due to the sign change of ψ_{2s} between r_a and r_b. This sign change is cancelled in the triplet case by the minus sign arising from the antisymmetrization. We may thus refer to this region of a smaller singlet probability relative to the triplet as $2s$-*conjugate Fermi hole* as will become apparent below.

The precise location of the $2s$-conjugate Fermi hole in the internal wave functions can be clearly seen by considering a cross section at $\phi_- = 0$ for the difference between the singlet and triplet probability densities of the $(2s)$ states of Fig. 7 (a) and (b). These cross sections are displayed in Fig. 10(a) and (b) corresponding, respectively, to Fig. 7(a) and (b) and represent cases with and without electron repulsion. The blue (light grey) and red (dark grey) contours indicate the region where the singlet wave

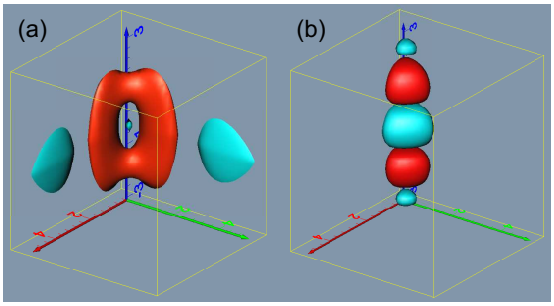

FIG. 10: (Color online) Difference between the probability density distributions of the $(2p)$ ^1P singlet and $(2p)$ ^3P triplet states in the internal space: (a) and (b) correspond to the cases with and without electron repulsion, respectively. See the caption to Fig. 7 for further details.

function has a larger probability than the corresponding triplet and vice versa. Therefore, the red contours in Fig. 9 represent the location of the $2s$-conjugate Fermi hole. As shown for the case without electron repulsion [cf. Fig. 10(b)], both the blue and red contours are located within a region of small r, $r_i < 2$ $(i = 1,2)$. The dotted diagonal line along which the electron repulsion potential diverges is defined by $r_1 = r_2$. Since the singlet and triplet wave functions are, respectively, symmetric and anti-symmetric with respect to the exchange of the r_1 and r_2 coordinates, the singlet wave function can have a finite density along this diagonal line while the triplet wave function cannot. For this reason the blue contours, representing the region where the singlet wave function has a larger density than the triplet, appear along this diagonal line. The region of these blue contours can be regarded as the location of the Fermi hole for the triplet wave function. On the other hand, since the electron density distributions calculated from these singlet and triplet wave functions *without electron repulsion* should be identical, the smaller probability density in the triplet wave function due to the Fermi hole should be balanced by a decrease in the singlet probability density in the region where the Fermi hole is located. This decrease in the singlet probability density corresponds to the $2s$-conjugate Fermi hole that is indicated by the red contours in Fig. 10(b). Therefore, the $2s$-conjugate Fermi hole and the genuine Fermi hole always appear as a pair since both of them have their origin in the antisymmetrization of the total wave functions. One may be apprehensive about this pairwise appearance of the genuine and the $2s$-conjugate Fermi holes since the latter requires a node in the orbitals to appear as described above while the Fermi hole does not require any such constraint. It is noted, however, that the Fermi hole requires two differenct orbitals since it appears only in the triplet wave function. Therefore, the number of nodes in the respective orbitals should differ. This guarantees the appearance of a $2s$-conjugate Fermi hole.

Once the electron repulsion potential is accounted for, the probability density distribution displayed in

Fig. 10(b) for the case without electron repulsion is spread towards large r_i (i = 1,2) values thus avoiding a strong potential barrier due to the electron repulsion along the diagonal line. The resulting distribution, shown in Fig. 10(a), still has a $2s$-conjugate Fermi hole in the range $0.5 < r_i < 2.5$, indicated by the red contours, while the size of the Fermi hole is significantly reduced along the diagonal line indicated by blue contours close to the origin. However, new blue contours in the range of $r_i >$ 2.8 appear instead. These blue contours in the range of large r_i represent a singlet probability that has migrated from the original small r_i region. Due to the presence of the $2s$-conjugate Fermi hole in the region of intermediate r_i ($0.5 < r_i < 2.5$), the singlet probability migrating out of the region of small r_i cannot accumulate in the intermediate region but has to move further away from the nucleus. This results in a broader electron density distribution for the singlet wave function. Further, since the blue contours in the region of large r_i displayed in Fig. 10 (a), representing the migrated singlet probability, is also apart from the diagonal line of the electron repulsion, the singlet wave function has a smaller electron repulsion energy than the corresponding triplet wave function.

A similar argument can be applied to the ($2p$) singlet-triplet pair although their *$2p$-conjugate Fermi hole* has a different topological structure in the internal space as displayed in Fig. 8. Indeed, unlike the $2s$ orbital, the $2p$ orbital is nodeless along the radial r coordinate. Therefore, it is its angular part that plays the key role. Similarly as for the ($2s$) singlet-triplet pair the orbital part of the ($2p$) wave functions can be written in a single-determinant approximation as

$$\Psi^{\pm}_{2p} = \frac{1}{\sqrt{4\pi}}[\psi_{1s}(r_1)\psi_{2p}(r_2)e^{i\phi_2} \pm \psi_{2p}(r_1)e^{i\phi_1}\psi_{1s}(r_2)], \tag{9}$$

where Ψ^{+}_{2p} and Ψ^{-}_{2p} represent singlet and triplet wave functions. These wave functions correspond to one component of the ($2p$) state with a positive orbital angular momentum of $L = 1$. There is of course another component with $L = -1$ but it yields the same internal wave function as does the other component. Therefore it is sufficient to consider the case of $L = 1$. By transforming the independent polar coordinates (ϕ_1, ϕ_2) into the symmetric and anti-symmetric coordinates (ϕ_+, ϕ_-), the square of the $|\Psi^{\pm}_{2p}|$ wave functions becomes

$$\begin{aligned}|\Psi^{\pm}_{2p}|^2 \;=\; & \frac{1}{4\pi}\left[|\psi_{1s}(r_1)|^2|\psi_{2p}(r_2)|^2 + |\psi_{2p}(r_1)|^2|\psi_{1s}(r_2)|^2\right. \\ & \left.\pm 2\psi_{1s}(r_1)\psi_{2p}(r_1)\psi_{1s}(r_2)\psi_{2p}(r_2)\cos 2\phi_-\right], \end{aligned}\tag{10}$$

which does not depend on the ϕ_+ coordinate. Multiplying the factor $4(\pi - |\phi_-|)$ due to the angular volume element, as described in Sec. II, the wave functions of Eq. (10) become the internal wave functions $|\Psi^{\rm norm}_{\rm int,2p}|^2$. By choosing the spatial region defined by $\phi_- = 0, \pm\pi$ with $r_1 = r_2$, where the electron repulsion potential diverges, the triplet probability density $|\Psi^{-}_{2p}|^2$ becomes zero while the singlet density $|\Psi^{+}_{2p}|^2$ has a finite amplitude. This indicates clearly the existence of Fermi holes in this region. On the other hand, the singlet density $|\Psi^{+}_{2p}|^2$ becomes in turn zero at $\phi_- = \pm\pi/2$ with $r_1 = r_2$ while the triplet density $|\Psi^{-}_{2p}|^2$ has a finite amplitude. This indicates that there exist $2p$-conjugate Fermi holes in this region of the internal space. The location of these $2p$-conjugate Fermi holes, as well as of the genuine Fermi holes, in the internal space for the zeroth order wave functions of Eq. (9) can be seen in Fig. 8(b) where the difference in probability densities between the singlet and triplet wave functions without electron repulsion has been displayed. The blue and red surfaces in Fig. 8, representing, respectively, the regions where the singlet wave function has a larger probability than the triplet, and vice versa, are located in the region centered at small r_i (i = 1,2) and $\phi_- = 0, \pm\pi$ for the former and $\phi_- = \pm\pi/2$ for the latter, respectively, as has been reasoned on the basis of Eq. (10).

As explained in the case of the ($2s$) singlet-triplet pair, the conjugate and the genuine Fermi holes occupy the same r_i region when disregarding the electron repulsion, since in this case the singlet and triplet wave functions have the same radial electron density distribution. Once the electron repulsion potential is accounted for, the three 'poles' of the electron repulsion potential peaked at $\phi_- = 0, \pm\pi$ [cf. Fig. 6] penetrate exactly into the respective three blue surfaces of the Fermi holes and strongly push the singlet probability densities away from this region. The resulting distribution displayed in Fig. 8(a) shows that most of the density indicated by the blue surfaces has migrated from the original region of small r_i (i = 1,2) into the region of large r_i. Again, due to the presence of the $2p$-conjugate Fermi holes in the intermediate r_i region, the singlet probability migrating out of the original region of small r_i cannot accumulate in this region but has to move farther away from the nucleus. The resultant singlet wave function thus has a broader radial electron density distribution and a smaller electron repulsion energy than the counterpart triplet state. The present results for the ($2s$) and ($2p$) singlet-triplet pairs of states which create a conjugate Fermi hole suggest that the Hund multiplicity rule has a clear wave mechanical origin and cannot be explained at the classical level of theory.

E. He-like atomic ions

The origin of the Hund multiplicity rule in the 2D helium atom as presented in the preceding section will now be reaffirmed by extending our analysis to 2D He-like ions. As in the case of the 2D He atom the three energy differences ΔE, ΔE_1, and ΔE_2, corresponding, respectively, to the total, one-electron, and two-electron energies between the singlet-triplet pairs of the ($2s$) and ($2p$) states, have been calculated for different nuclear charges Z ($2 \le Z \le 10$) and are plotted in Fig. 11. The results

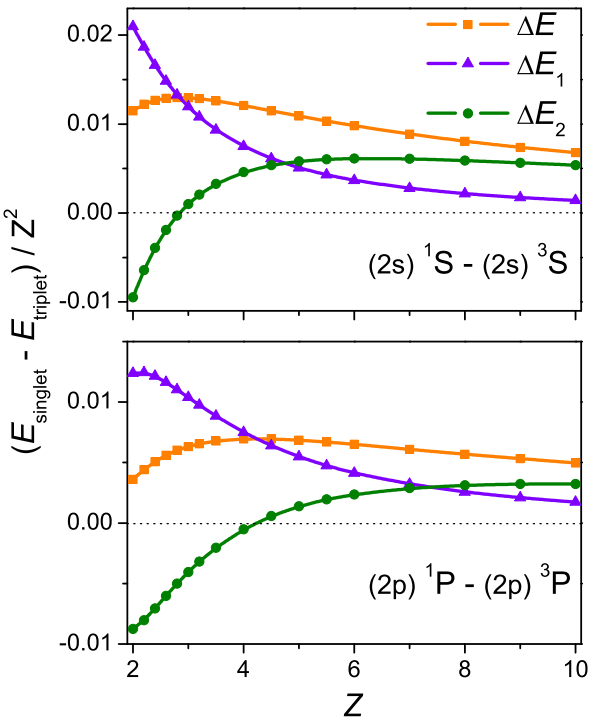

FIG. 11: (Color online) Energy differences between the $(2s)$ singlet-triplet pair (upper figure) and the $(2p)$ singlet-triplet pair (lower figure) of states of He-like ions for different nuclear charges Z. The difference in the total, one-electron, and two-electron energies is denoted by ΔE, ΔE_1, and ΔE_2, respectively.

for fractional values of the nuclear charge Z have been included also in this figure in order to study the trend of the energy differences as a function of Z. The energy differences are scaled by Z^2 so that the results for different values of Z can be easily compared. The total energy ΔE and its components ΔE_1 and ΔE_2 are represented in Fig. 11 by squares, triangles, and circles, respectively.

The two-electron energy difference ΔE_2 for both the $(2s)$ and $(2p)$ pairs of states is negative for small Z values that are close to the helium case of $Z = 2$. This indicates again a larger electron repulsion for the triplet. Similarly, the one-electron energy difference ΔE_1 is positive and overcompensates the negative ΔE_2 so that the triplet has a lower energy than the singlet. On the other hand, as Z increases ΔE_2 increases as well and becomes positive at $Z = 3$ for the $(2s)$ pair and for Z slightly larger than four also for the $(2p)$ pair. This is again consistent with the result known for the 3D helium like ions [27] for which ΔE_2 becomes positive for the (2s) pair at $Z = 3$ and for the (2p) pair at $Z = 4$. In the present case of 2D helium like ions ΔE_2 is still slightly negative for the $(2p)$ pair at $Z = 4$. For the corresponding 3D helium like ions it is slightly positive at $Z = 4$. Therefore, the general trend is basically the same. In contrast to the increasing ΔE_2 the one-electron energy difference ΔE_1 monotonically decreases with increasing Z. Thus, the energy differences ΔE_1 and ΔE_2 eventually cross in the range $4 < Z < 5$ for the $(2s)$ pair and $7 < Z < 8$ for the $(2p)$ pair. Finally, ΔE_1 approaches zero as Z further increases so that ΔE_2 approaches more and more ΔE. This indicates that for large values of Z the two-electron contribution to the singlet-triplet energy gap becomes dominant so that the interpretation of Hund's first rule based on Slater's early study [14] becomes more and more plausible.

The dominant effect of ΔE_2 over ΔE_1 that governs the singlet-triplet energy gap for large Z values may be easily understood by scaling the electron coordinates by the nuclear charge. By using the new coordinates $\vec{s}_i = Z\vec{r}_i$ $(i = 1{,}2)$ in the Hamiltonian (1) for a general nuclear charge Z we obtain

$$\mathcal{H}/Z^2 = \left[-\frac{1}{2}\sum_{i=1}^{2} \vec{\nabla}_{s,i} - \sum_{i=1}^{2} \frac{1}{|\vec{s}_i|} + \frac{1}{Z}\frac{1}{|\vec{s}_1 - \vec{s}_2|} \right], \quad (11)$$

where both sides of the equation have been divided by Z^2 so that the eigenenergies for different values of Z will be of the same order of magnitude and may be easily compared. As seen from Eq. (11) the one-electron part of the scaled Hamiltonian is identical for all Z so that the same one-electron orbitals and solutions result for all values Z when the interelectronic repulsion is disregarded. Furthermore, the interelectronic repulsion potential involves a factor inversely proportional to Z and this term is becoming less and less important relative to the kinetic and nuclear attraction energies as Z increases. This relative decrease in the electron repulsion potential manifests itself in a decrease of the size of the three 'poles' of the electron repulsion potential shown in Fig. 6 when the Z-scaled internal space (Zr_1, Zr_2, ϕ_-) is used. Moreover, since in this Z-scaled internal space the wave functions are identical for different Z when disregarding the electron repulsion, the effect of the electron repulsion potential term on the wave functions decreases with increasing Z.

The general trend of the energy differences between the singlet-triplet pairs of states, displayed in Fig. 11 for different Z, can be rationalized based on the previous discussion. For large values of Z (e.g., $Z \approx 10$) the three poles of the electron repulsion potential get small so that both the singlet and triplet wave functions will not differ significantly from those obtained *without* the electron repulsion term. This means that the electron density distribution of the singlet and triplet states will be nearly the same and will yield similar expectation values for the one-electron energies. On the other hand, as has been seen earlier in Figs. 3(a') and 4(a'), the singlet wave functions without electron repulsion have a significant probability density in the region $\phi_- = 0, \pm\pi$ with $r_1 = r_2$, where the electron repulsion potential diverges and the corresponding triplet wave functions have a node

in this region due to the Fermi hole. Thus, the singlet states should have a larger expectation value of the electron repulsion potential than the corresponding triplet states. Precisely for this reason the singlet-triplet energy gap is dominated in the large Z regime by the difference in the two-electron energies and the one-electron contribution is small as proved by the results displayed in Fig. 11. This dominance of the two-electron contribution corresponds more or less to the interpretation of Hund's first rule based on Slater's early study [14]. As the nuclear charge Z decreases, the three poles of the electron repulsion potential become more pronounced and cause larger changes of the internal wave functions. As a result, the probability density of the singlet wave function in the vicinity of the Fermi hole migrates into the region of large r_i (i = 1,2) values due to the existence of the *conjugate Fermi hole*, as explained in Sec. III C. The triplet wave function is modified more gently due to the Fermi hole. Due to the decrease in the probability density in the region of the Fermi hole for the singlet wave function, the electron repulsion in the singlet state becomes smaller and thus the energy difference in the two-electron energies between the corresponding singlet and triplet states, ΔE_2, decreases. On the other hand, since the singlet wave function acquires an increased probability density in the region of large r_i values, the potential energy increases stronger due to the nuclear attraction potential than in case of the counterpart triplet wave function. Therefore, as Z decreases the two-electron contribution to the singlet-triplet energy gap becomes smaller while the one-electron contribution becomes larger as displayed in Fig. 11. Finally, as Z further decreases towards the helium case the three poles of the electron repulsion potential become so strong that a major part of the singlet probability density around the origin migrates towards the region of large r_i. Since the migrated probability is located away from the nucleus as well as from the three poles of the electron repulsion potential as displayed in Figs. 7 and 8, the singlet state has a broader electron density distribution and a smaller electron repulsion potential than its counterpart triplet state. In other words, for small Z values close to the helium case the triplet is characterized by a more compact electron density distribution and a larger electron repulsion.

IV. SUMMARY

In the present study of the origin of Hund's multiplicity rule in the excited states of the 2D helium atom we have employed the full configuration interaction method to generate the energy spectrum and to partition the total energy into its one-electron and two-electron components. The differences of these quantities for the singlet-triplet pairs of states possess similar characteristics as are known for the corresponding 3D helium atom. This supports our attempt to provide new fundamental insight into the origin of the Hund multiplicity rule on the basis of the results for the 2D helium atom that is made possible by the lower dimensionality of our model. It must be emphasized that the dimension of the internal space of our 2D helium atom is the same as that of the corresponding 3D helium atom. This coincidence of the dimensionality of the internal space of the 2D and 3D systems is usually not the case for more than three electrons but it happens for two-electron systems having circular and spherical symmetries for the 2D and 3D systems, respectively. This is one of the main reasons why we have chosen the 2D helium atom for our investigation of the origin of Hund's multiplicity rule.

In our analysis we have extracted first the internal part of the wave functions for the ($2s$) and ($2p$) singlet-triplet pair of states from the CI wave functions and visualized them in the *internal space* (r_1, r_2, ϕ_-). This has provided us with new insight into the structure of the relevant wave functions which in turn has enabled us to rationalize the well-known characteristics of helium, namely, a more compact electron density distribution and larger electron repulsion in the triplet states than in the corresponding singlet states. The probability density distributions along the internal angle ϕ_- obtained by integrating the internal wave functions over the radial coordinates (r_1, r_2) closely follow the *statistical distribution*. This indicates that there is little preference for the two electrons to take a particular inter-electron angle $\angle$(e$-\alpha-$e). We have visualized also the electron repulsion potential in the internal space which is characterized by three striking poles peaked at $\phi_- = 0, \pm\pi$ penetrating exactly into the spatial region defined by the Fermi hole. In order to identify the role played by the electron repulsion potential, the internal wave functions *without* electron repulsion have been generated and visualized also. A careful examination of these zero-order internal wave functions without the electron repulsion implies the existence of a region in the internal space in the immediate vicinity of the Fermi hole where the singlet wave function has a smaller probability density than the counterpart triplet wave function. We refer to it as the *conjugate Fermi hole*. It is shown to be a consequence of the antisymmetrization of the total wave function and thus has the same origin as the genuine Fermi hole.

The internal wave functions of the singlet and triplet states obtained by ignoring the electron repulsion undergo distinct changes once the electron repulsion is accounted for. The three poles of the electron repulsion potential exactly penetrate into the region of a Fermi hole. Therefore the triplet wave function that has a rather insignificant probability in the vicinity of this Fermi hole is less affected by these poles than the singlet wave function. This explains why, generally, the interelectronic repulsion plays a more important role in the singlet state than in the counterpart triplet state. In contrast, the probability density of the singlet wave function has to migrate from this region in order to avoid the strong potential poles of the electron repulsion. This migrating probability density of the singlet wave function has to avoid

also the region around the conjugate Fermi hole since the singlet probability cannot penetrate into the conjugate Fermi hole. Consequently, the migrating probability density of the singlet state has to move far away from its original region close to the nucleus. Thus, the resultant singlet wave function has a probability distribution extended into the region of large r_i ($i = 1,2$) values which in turn makes the radial electron density distribution of the singlet state more diffuse than that of the counterpart triplet state. Furthermore, since the singlet probability that is located in the region of large r_i is now further away from both the poles of the electron repulsion and from the nucleus, the singlet state has a smaller electron repulsion and a smaller energy decrease due to the nuclear attraction potential than the triplet state. In other words, the counterpart triplet state possesses a more compact electron density distribution, a larger electron repulsion and a larger energy decrease due to the nuclear attraction than does the corresponding singlet state.

V. AKNOWLEDGEMENT

The present study has been supported in parts by Grants-in-Aid for Scientific Research (No 20750018) from the Ministry of Education, Culture, Sports, Science and Technology (MEXT) and by Nihon University Strategic Projects for Academic Research. One of us (J.P.) gratefully acknowledges the continued support by the National Sciences and Engineering Research Council of Canada and two of us (T.S. and G.H.F.D.) would like to thank the Department of Applied Mathematics of the University of Waterloo for its hospitality.

[1] F. Hund, Z. Phys. **33**, 345 (1925).
[2] F. Hund, Z. Phys. **34**, 296 (1925).
[3] F. Hund, *Linienspektren und periodisches System der Elemente* (Springer, Berlin, 1927), pp. 98, 124.
[4] H. Rechenberg, in *Hundert Jahre Friedrich Hund*, edited by M. Schroeder (VandenHoeck and Ruprecht, Goettingen, 1996), Nachrichten der Akademie der Wissenschaften in Göttingen. II Mathematisch-Physikalische Klasse, pp. 4–32.
[5] G. Herzberg, *Atomic Spectra and Atomic Structure* (Dover, New York, 1944), p. 135.
[6] L. Szasz, *The Electronic Structure of Atoms* (Wiley, New York, 1992), p. 52.
[7] B. W. Shore and D. H. Menzel, *Principles of Atomic Spectra* (Wiley, New York, 1968), p. 101.
[8] H. Friedrich, *Theoretical Atomic Physics* (Springer, Berlin, 2006), p. 105.
[9] G. Herzberg, *Molecular Spectra and Molecular Structure, Vol. 1, Spectra of Diatomic Molecules* (Van Nostrand, New York, 1950), p. 335, 2nd ed.
[10] J. P. Colpa and R. E. Brown, Mol. Phys. **26**, 1453 (1973).
[11] L. Kouwenhoven, T. H. Oosterkamp, M. W. S. Danoesastro, M. Eto, D. G. Austing, T. Honda, and S. Tarucha, Science **278**, 1788 (1997).
[12] S. Bednarek, B. Szafran, and J. Adamowski, Phys. Rev. B **59**, 13036 (1999).
[13] P. Matagne, J. P. Leburton, D. G. Austing, and S. Tarucha, Physica E **13**, 679 (2002).
[14] J. C. Slater, Phys. Rev. **34**, 1293 (1929).
[15] E. R. Davidson, J. Chem. Phys. **41**, 656 (1964).
[16] E. R. Davidson, J. Chem. Phys. **42**, 4199 (1965).
[17] R. P. Messmer and F. W. Birss, J. Phys. Chem. **73**, 2085 (1969).
[18] D. A. Kohl, J. Chem. Phys. **56**, 4236 (1972).
[19] J. Katriel, Phys. Rev. A **5**, 1990 (1972).
[20] J. Katriel, Theoret. Chim. Acta **23**, 309 (1972).
[21] J. Katriel, Theoret. Chim. Acta **26**, 163 (1972).
[22] J. Katriel and R. Pauncz, Adv. Quantum Chem. **10**, 143 (1977).
[23] R. J. Boyd and C. A. Coulson, J. Phys. B **6**, 782 (1973).
[24] R. J. Boyd and C. A. Coulson, J. Phys. B **7**, 1805 (1974).
[25] R. J. Boyd, Nature **310**, 480 (1984).
[26] J. P. Colpa, A. J. Thakkar, J. V. H. Smith, and P. Randle, Mol. Phys. **29**, 1861 (1975).
[27] P. E. Regier and A. J. Thakkar, J. Phys. B **17**, 3391 (1984).
[28] T. Koga, H. Matsuyama, J. S. Dehesa, and A. J. Thakkar, J. Chem. Phys. **110**, 5763 (1999).
[29] I. Shim and J. P. Dahl, Theor. Chim. Acta. **48**, 165 (1978).
[30] K. Hongo, R. Maezono, Y. Kawazoe, H. Yasuhara, M. D. Towler, and R. J. Needs, J. Chem. Phys. **121**, 7144 (2004).
[31] T. Oyamada, K. Hongo, Y. Kawazoe, and H. Yasuhara, J. Chem. Phys. **125**, 014101 (2006).
[32] T. Oyamada, K. Hongo, Y. Kawazoe, and H. Yasuhara, J. Chem. Phys. **133**, 164113 (2010).
[33] Y. Sajeev, M. Sindelka, and N. Moiseyev, J. Chem. Phys. **128**, 061101 (2008).
[34] T. Sako, J. Paldus, and G. H. F. Diercksen, Phys. Rev. A **81**, 022501 (2010).
[35] C. M. Reeves, J. Chem. Phys. **39**, 1 (1963).
[36] C. M. Reeves and M. C. Harrison, J. Chem. Phys. **39**, 11 (1963).
[37] S. Wilson, *Electron Crrelation in Molecules* (Oxford: Clarendon, 1984).
[38] R. S. Berry and J. L. Krause, Adv. Chem. Phys. **70**, 35 (1988).
[39] B. G. Wybourne, *Classical Groups for Physicists* (John Wiley & Sons, New York, 1974), p. 214.